OPEN ACCESS

Journal of Petroleum and Gas Engineering

March 2019
ISSN 2141-2677
DOI: 10.5897/JPGE
www.academicjournals.org

ACADEMIC JOURNALS
expand your knowledge

About JPGE

Journal of Petroleum and Gas Engineering (JPGE) is a peer reviewed journal. The journal is published per article and covers all areas of the subject such as: Petroleum geology, Reservoir simulation, Enhanced oil recovery, subsurface analysis and Drilling technology.

Open Access Policy

Open Access is a publication model that enables the dissemination of research articles to the global community without restriction through the internet. All articles published under open access can be accessed by anyone with internet connection.

The Journal of Petroleum and Gas Engineering is an Open Access journal. Abstracts and full texts of all articles published in this journal are freely accessible to everyone immediately after publication without any form of restriction.

Article License

Memberships and Standards

Academic Journals strongly supports the Open Access initiative. Abstracts and full texts of all articles published by Academic Journals are freely accessible to everyone immediately after publication.

All articles published by Academic Journals are licensed under the Creative Commons Attribution 4.0 International License (CC BY 4.0). This permits anyone to copy, redistribute, remix, transmit and adapt the work provided the original work and source is appropriately cited.

Crossref is an association of scholarly publishers that developed Digital Object Identification (DOI) system for the unique identification published materials. Academic Journals is a member of Crossref and uses the DOI system. All articles published by Academic Journals are issued DOI.

Similarity Check powered by iThenticate is an initiative started by CrossRef to help its members actively engage in efforts to prevent scholarly and professional plagiarism. Academic Journals is a member of Similarity Check.

CrossRef Cited-by Linking (formerly Forward Linking) is a service that allows you to discover how your publications are being cited and to incorporate that information into your online publication platform. Academic Journals is a member of CrossRef Cited-by.

Academic Journals is a member of the International Digital Publishing Forum (IDPF). The IDPF is the global trade and standards organization dedicated to the development and promotion of electronic publishing and content consumption.

COUNTER (Counting Online Usage of Networked Electronic Resources) is an international initiative serving librarians, publishers and intermediaries by setting standards that facilitate the recording and reporting of online usage statistics in a consistent, credible and compatible way. Academic Journals is a member of COUNTER

Portico is a digital preservation service provided by ITHAKA, a not-for-profit organization with a mission to help the academic community use digital technologies to preserve the scholarly record and to advance research and teaching in sustainable ways.

Academic Journals is committed to the long-term preservation of its content and uses Portico

Academic Journals provides an OAI-PMH(Open Archives Initiatives Protocol for Metadata Harvesting) interface for metadata harvesting.

Contact

Editorial Office: jpge@academicjournals.org

Help Desk: helpdesk@academicjournals.org

Website: http://www.academicjournals.org/journal/ JPGE

Submit manuscript online http://ms.academicjournals.org

Academic Journals

73023 Victoria Island, Lagos, Nigeria

ICEA Building, 17th Floor, Kenyatta Avenue, Nairobi, Kenya

Editors

Table of Content

Vol. 10(2), pp. 14-22, March 2019
DOI: 10.5897/JPGE2018.0299
Article Number: 533242B60367
ISSN: 2141-2677

http://www.academicjournals.org/JPGE

ACADEMIC JOURNALS

Journal of Petroleum and Gas Engineering

Full Length Research Paper

Prediction of the water saturation around wells with bottom water drive using artificial neural networks

Muhammad Alrumah[1*] and Turgay Ertekin[2]

[1]Public authority for Applied Education and Training, Kuwait.
[2]Institute for Turgay Ertekin is Pennsylvania State University, USA.

Received 1 October, 2018; Accepted 28 January, 2019

This study is concerned with the water coning phenomenon that takes place around production wells of hydrocarbon reservoirs. In this paper, the development of artificial neural networks to predict the water saturation buildup around vertical and horizontal wells with a good level of accuracy is described. In the development of expert systems, it is assumed that water encroachment originates from an active aquifer which is located under the hydrocarbon reservoir (reservoir with bottom water drive). A high-fidelity numerical model is utilized in generating training data sets that are used in structuring and training the artificial neural networks. The artificial expert systems that are developed in this paper are universal and are capable of predicting the change of water saturation around the wellbore as a function of time and the prediction process is faster than a reservoir simulator and requires less data, which saves time and effort. With the help of these models, it will be possible to predict the position of high water saturation zones around the wellbore ahead of time so that remedial actions such as closing the perforations that produce the water can be implemented on a timely basis.

Key words: Bottom water drive, water coning, neural network, water saturation, vertical well, horizontal well.

INTRODUCTION

Many hydrocarbon reservoirs contain an active water aquifer. The drilled wells are always completed to produce only hydrocarbons. As oil production continues, water starts to appear in the wellbore. This water is undesirable as its presence around the wellbore decreases the well productivity and needs more facilities to be handled, treated and disposed of at the surface resulting in extra investments and operating costs. The height of the water cone stops increasing if the upward dynamic flow forces become equal to the downward gravitational forces. The water will be produced once the height of the water reaches the wellbore. By continuing to produce the hydrocarbon with water, formation around the wellbore will be saturated with water in the shape of a cone, a phenomenon that is referred to as water coning. This study analyzes the water coning phenomenon. The water coning behavior has significant importance in hydrocarbon production, and the ability to predict its future behavior will improve and help in better managing reservoirs experiencing water encroachment. The behavior of the water coning in an oil reservoir is predicted successfully using Artificial Neural Networks (ANN) by predicting the change of the water saturation distribution in the reservoir over time, and the prediction

*Corresponding author. E-mail: mk.alrumah@paaet.edu.kw.

process is faster than a reservoir simulator and requires less data, which saves time and effort. The developed neural networks were designed to be used for vertical and horizontal wells in communication with a bottom water aquifer. These developed neural networks can be useful in optimizing production by finding the optimum perforation interval or the optimum production rate to delay the water production.

The first paper discussed the water coning phenomenon and its physics was done by Muskat and Wyckoff (1935). Muskat and Wyckoff (1935) indicated that some of the factors that affect the water coning are production rate and length of perforated interval. Others performed numerical studies on the effects of various parameters on water coning in vertical wells (Blades and Stright, 1975; Byrne and Morse, 1973; Mungan, 1975). Also, Kuo (1983) studied the effects of various parameters on water coning in vertical wells, and developed correlations to predict critical rate, breakthrough time, and watercut after water production. Yang and Wattenbarger (Yang and Wattenbarger, 1991) studied the water coning effects in vertical and horizontal wells and developed a method to calculate the critical rate, break- through time, and the water-oil ratio after breakthrough. Van (1994) investigated the water coning behavior for a fractured reservoir in a vertical well and studied various parameters and their effects on water coning. Helle and Bhatt (2002) developed artificial neural networks that predict the underground fluids (water, oil and gas) and their partial saturation directly from the well logs. Shokir (2004) presented new artificial neural networks that predict water saturation in shaly formation using the well log data and the core data as the inputs. Al-Bulushi et al. (2009) developed artificial neural network based models to predict water saturation from well log data and core data. Mahmoudi and Mahmoudi (2014) developed artificial neural network that predicts porosity and water saturation of an Iranian oil field using well logs as an input data. Zendehboudi et al. (2014) developed a hybrid artificial neural network with particle swarm optimization to estimate breakthrough time and critical production rate for fractured system. Hamada et al. (2015) used neural network, optimized by particle swarm optimization, to determine the parameters of Archie's formula, and then use the formula to calculate water saturation. Finally, Gholanlo et al. (2016) used radial basis function neural network improved by genetic algorithm to predict formation water saturation using conventional well-logging data. Gharib et al. (2018) developed artificial neural network to predict water saturation and porosity for shaly sand using core and log data. Baziar et al. (2018) performed a comparative study using four intelligent methods to determine water saturation in a tight gas sandstone reservoir and the methods are support vector machine, multilayer perceptron neural network, decision tree forest, and tree boost. Alimoradi et al. (2011) pointed out that one of the most important parameters in reservoir characterization procedure is water saturation, and the aim of this study is the future prediction performance of water saturation.

MODELS DEVELOPMENT

Numerical model

Data used to train the artificial neural networks were generated from a numerical reservoir simulation model. Two reservoir numerical models were implemented in radial and rectangular coordinates. The reservoir properties are assumed to be homogeneous and isotropic. In terms of fluid properties, the reservoir conditions are assumed to be above the bubblepoint pressure to ensure that no free gas is present in the reservoir. Furthermore, capillary forces were ignored assuming no transition zone. The reservoirs are assumed to be horizontal with uniform thicknesses. The radial reservoir model was used to generate data for vertical wells and the rectangular reservoir model was used to generate data for horizontal wells. The gridding for the radial system was in three dimensions, where the number of grid blocks was 30×1×25. The thickness of all the grid blocks is equal and the spacing of grids in the r-direction was designed according to the following equation:

$$r_i = r_w \left(\frac{r_e}{r_w}\right)^{\backslash(i/30)} \quad (1)$$

The rectangular reservoir gridding was 25×25×15 with $\Delta x = \Delta y =$ 61 m. The reservoir properties for the radial and the rectangular models are tabulated in Tables 1 and 2. For the vertical well scenario, six key parameters were selected to be changed to create different oil reservoirs. The parameters with their ranges are shown in Table 3 for the vertical well scenarios and in Table 4 for the horizontal well scenarios.

Artificial neural network vertical well scenario

A total of 233 data sets were generated randomly. Each combination was used to create a new reservoir model. All of the runs were designed for 10 years. The water saturation data, for all the blocks as generated by the simulation runs, were collected and prepared for the ANN training process. The ANN used for training is a feedforward network. The principal inputs are six parameters, which are:

(1) Oil density (ρ_O),
(2) Oil viscosity (μ_O),
(3) Vertical permeability (k_V),
(4) Total liquid flow rate (q_L),
(5) Reservoir thickness (h),
(6) Open interval to the flow (h_p).

The outputs are the water saturation values for all the blocks in the reservoir model at the end of each year. The 233 scenarios were divided into three sets; 210 scenarios were used for training, 11 for validation and 12 for blind

Table 1. Reservoir properties for the radial system.

Porosity (φ)	0.25
k_r, m^2	500×10^{-15}
Reservoir radius (r_e), m	1,829
Oil formation volume factor, Rm^3/Sm^3	1.0
Oil compressibility (c_O), MPa^{-1}	145×10^{-6}
Initial pressure (p_i), MPa	34.5
Temperature, °C	54
Initial oil saturation (S_{oi})	1.00

Table 2. Reservoir properties for the rectangular system.

Porosity (φ)	0.25
k_X, m^2	500×10^{-15}
k_y, m^2	500×10^{-15}
Reservoir length, m	1,524
Reservoir width, m	1,524
Oil formation volume factor, Rm^3/Sm^3	1.0
Oil compressibility (c_O), MPa^{-1}	145×10^{-6}
Initial pressure (p_i), MPa	34.5
Temperature, °C	54
Initial oil saturation (S_{oi})	1.00

Table 3. The selected reservoir properties were changed within their ranges for the vertical well study.

S/N	Parameter	Range
1	Oil density (ρ_O), kg/m^3	769 - 929
2	Oil viscosity (μ_O), cp	1 - 10
3	Vertical permeability (k_V), m^2	5×10^{-15} - 500×10^{-15}
4	Total liquid fl w rate (q_L), m^3/Day	79.5 - 1,590
5	Reservoir thickness (h), m	7.6 - 76
6	open to fl w interval of pay zone (h_p), m	0.04 - 0.96 h

testing. Training and validation data are used in the training of the ANN and the testing data are only introduced to the network after the end of the training process to test the new ANN. Training the neural network started by including all water saturation values for all the blocks of each reservoir, which will produce a network that can predict the water saturation for the entire reservoir. However, this did not result in a capable network that could predict the water saturation values with a good level of accuracy. The next trial was to reduce the amount of data to simplify the problem for the neural network, and at the same time not to generate a large catalog of neural networks. The volume of data was reduced more to simplify the problem by taking the data for only one layer instead of the 25 layers, but these efforts were not successful once again. Then again, the data was reduced by taking the data of a single layer and considering only the 6 blocks. This time, a good network was generated and the absolute error was less than 10% for all the predicted water saturation values. The absolute error is calculated using the following equation:

$$Error = |S_W - S_W(ANN)| \quad (2)$$

After succeeding in designing a satisfactory network, the goal now is to increase the complexity of the problem and reduce the number of the networks needed to predict the water

Table 4. The selected reservoir properties were changed within their ranges for the horizontal well study.

S/N	Parameter	Range
1	Oil density (ρ_O), kg/m^3	769 - 929
2	Oil viscosity (μ_O), cp	1 - 10
3	Vertical permeability (k_V), m^2	5×10^{-15} - 500×10^{-15}
4	Total liquid fl w rate (q_L), m^3/Day	79.5 - 1,590
5	Reservoir thickness (h), m	4.6 - 73
6	Depth of the horizontal well from top of formation (h_d), m	0.067 - 0.53 h
7	Length of the horizontal well (h_L), m	183 - 1,036

saturation for the reservoir.

The complexity was increased by including the data for the 10 years and not only for one year. The produced networks were good. Increasing the number of blocks to 16 blocks was tried, but the efforts were not successful. At the end, 25 networks were considered, where each network predicts the water saturation for each layer at the end of each year for 10 years.

Horizontal well scenario

A total of 314 combinations were generated randomly and for each combination, a reservoir was created. The horizontal well was always placed in the center of the square reservoir. This created a symmetry, which reduces the amount of data to be considered, and in return, will reduce the time needed to train the neural network.

After running the numerical simulation for all the 314 reservoirs for 10 years, water saturation data was collected and prepared for training the neural networks.

The input list required to generate the blocks' water saturations as outputs, contains seven parameters, which are:

(1) Oil density (ρ_O),
(2) Oil viscosity (μ_O),
(3) Vertical permeability (k_V),
(4) Total liquid flo w rate (q_L),
(5) Reservoir thickness (h),
(6) Depth of the horizontal well (h_d),
(7) Length of the horizontal well (h_L).

The data collected was only from the vertical plane (x-z plane) which contains the horizontal well. The water saturation for each block at the end of each year was collected. Training the neural network using the water saturation values for the blocks in a single column, produced 13 different neural networks. The data for the 314 reservoirs were divided into 3 groups: 284 for training, 15 for validation, and 15 for blind testing. The resulting ANN is considered good when the predicted water saturation of the testing data has an absolute error of less than 10% for all values. The structure of the ANN was selected after trial and error. The network with the lowest error found was the feedforward network. The learning function with the lowest error was the gradient descent with momentum weight and bias learning function. The training function with the lowest error was the conjugate gradient backpropagation with Polak-Ribiére updates. The transfer functions which showed the lowest error was the hyperbolic tangent sigmoid transfer function. The neural network structure consists of the input and the output layers and two or more hidden layers. In each layer (input, output and hidden), the number of neurons must be specified. The number of neurons in the input layer is 7. The number of neurons in the output layer is 150. A table of 150 neurons is required because each column has 15 blocks and the water saturation value for a single block was taken at the end of each year for 10 years.

RESULTS AND DISCUSSION

Vertical well

As explained earlier, in this case, 25 ANN were created. They were tested using data from 12 different reservoirs. The average absolute error was less than 10% for all the layers of all 12 reservoirs. The structure of all the networks consists of one input layer, one output layer and two hidden layers. For each network, the outputs were the water saturation values for the blocks at the end of each year, for 10 years. Figure 1 shows the structure of the generated ANN for the first layer. The network has 6 inputs in the input layer, 46 neurons in the first hidden layer, 37 neurons in the second hidden layer, and 60 outputs in the output layer. The average absolute error for each layer of the reservoirs is found to be between 0.07 and 1.67%. Two reservoirs (reservoir #230 and #233) were selected, from the reservoirs used to test the generated ANN, to show the capability of the ANN in predicting the water saturation. Reservoir #230 has the highest average absolute error (Figure 3c), among the 12 tested reservoirs, for the predicted water saturation values, and reservoir #233 was randomly selected. Figure 2a shows the surface map of the water saturation distribution for reservoir #233 from numerical simulation data. Figure 2b shows the same water saturation distribution but with predicted data from ANN. The prediction has a very low error, and the water cone shape is captured clearly. Figure 2c shows the absolute error on a surface map to give a better way of visualizing the error and its location. The highest error is 5.9% and it is observed in a very small area. Figure 3a is for the

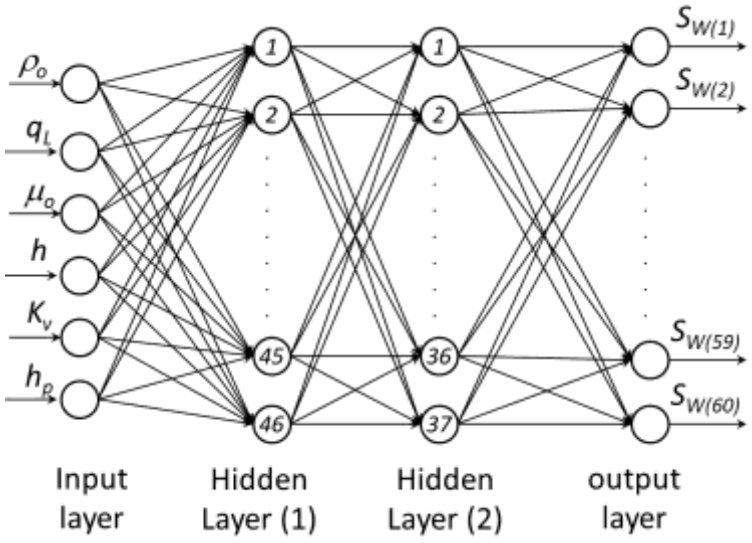

Figure 1. ANN structure generated for the fi layer for the vertical well.

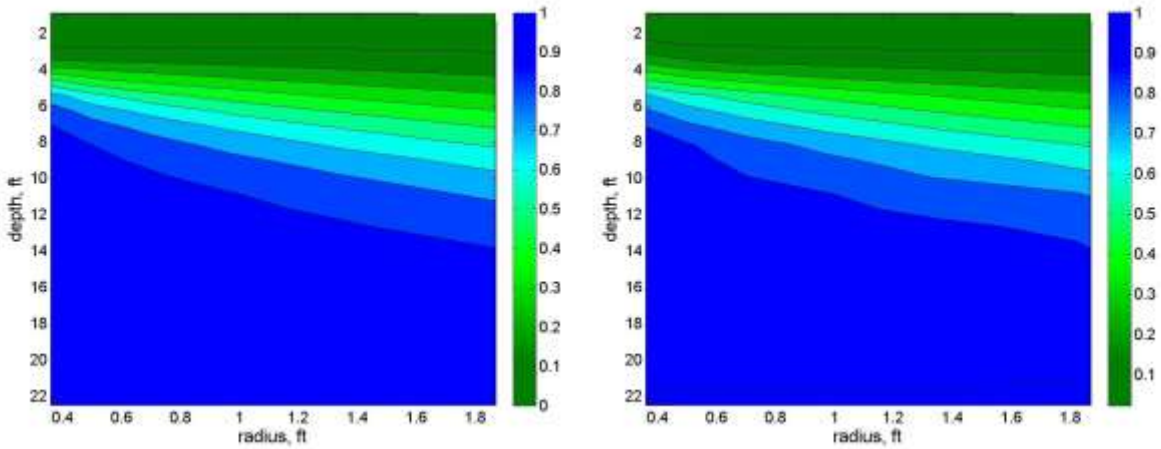

(a) Numerical simulation

(b) Artificial neural network

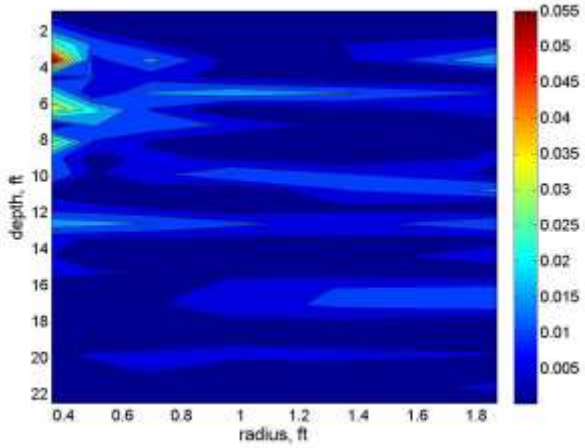

(c) Absolute error

Figure 2. Surface map of S_W for reservoir #233 at the end of the 6th year.

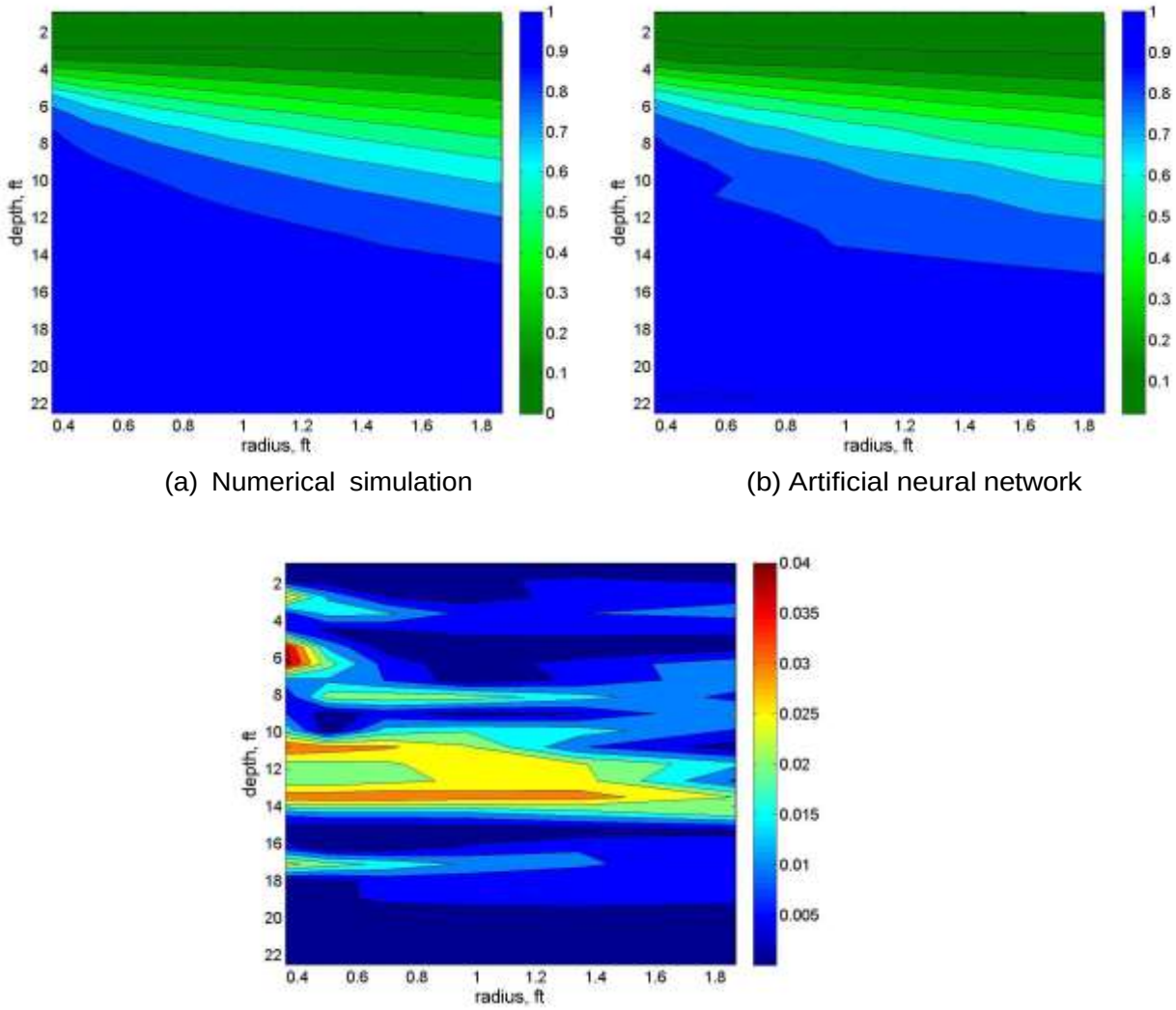

(a) Numerical simulation

(b) Artificial neural network

(c) Absolute error

Figure 3. Surface map of S_W for reservoir #230 at the end of the 5th year.

surface map for reservoir #230 for the water saturation using the data from the numerical simulation. Figure 3b is the surface map for the same reservoir using data predicted with the ANN. Figure 3c shows the absolute error. Prediction for this reservoir has the highest error among the 12 reservoirs used for testing, but the shape of the cone has developed, which is clearly visible from the ANN model.

Horizontal well

Twelve ANNs were generated. Each network predicts the water saturation for each column. The structure of all the networks consists of one input layer, one output layer and 2 or 3 or 4 hidden layers. The output layer has the water saturation values for the blocks at the end of each year, for 10 years.

Figure 4 shows the structure of the generated ANN for the first column. The network has 7 input neurons, 31 neurons in the first hidden layer, 37 neurons in the second hidden layer, and 150 neurons in the output layer. The average absolute error encountered in the 15 reservoirs was found to be very low (between 0.34 and 2.72%).

Fifteen reservoirs were tested using the neural networks developed in this study and two reservoirs were selected to illustrate the results of the ANN predictions. The two selected reservoirs are reservoirs #8 and #10. Figure 5a shows the surface map of reservoir #8 of water saturation from numerical simulation. The horizontal well is at a depth of 12.5 m and the horizontal section is 1,036 m long extending from 244 to 1,280 m. Figure 5b shows the surface map of the same reservoir with water

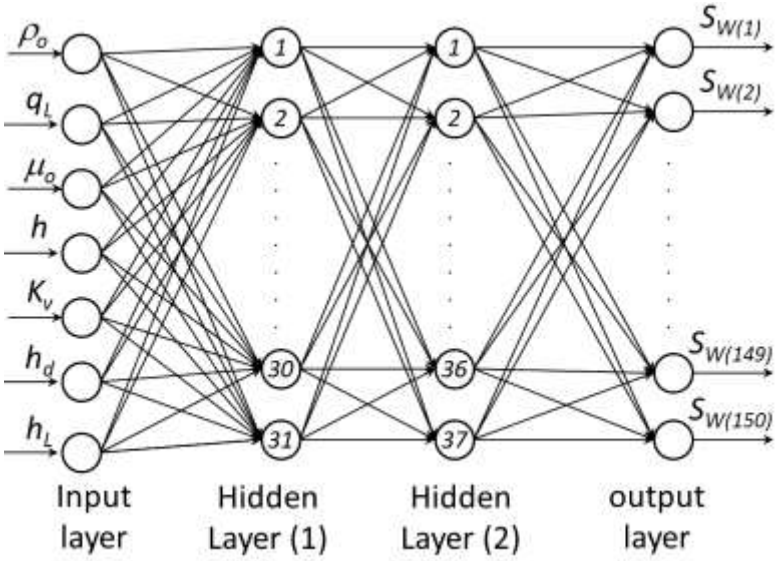

Figure 4. ANN structure generated for the fi column for the horizontal well.

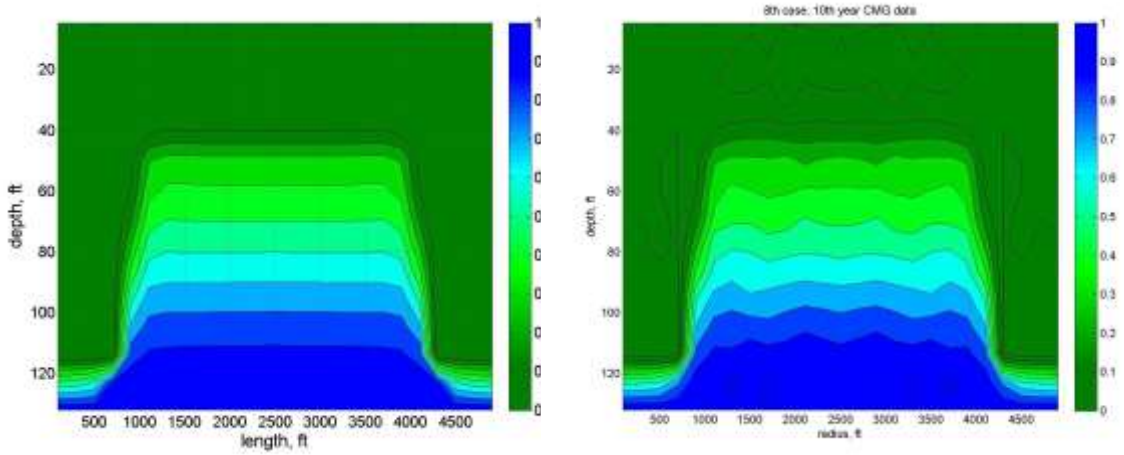

(a) Numerical simulation (b) Artificial neural network

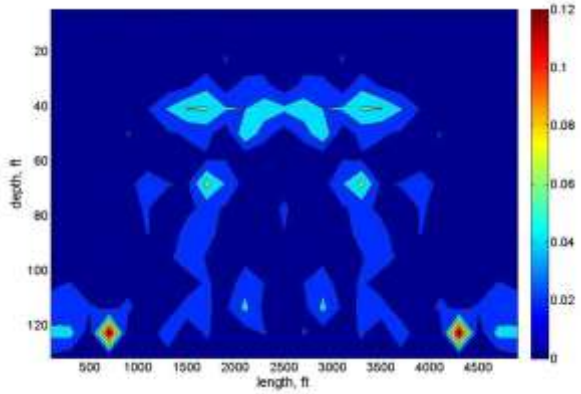

(c) Absolute error

Figure 5. Surface map of S_W for reservoir #8 at the end of the 10th year.

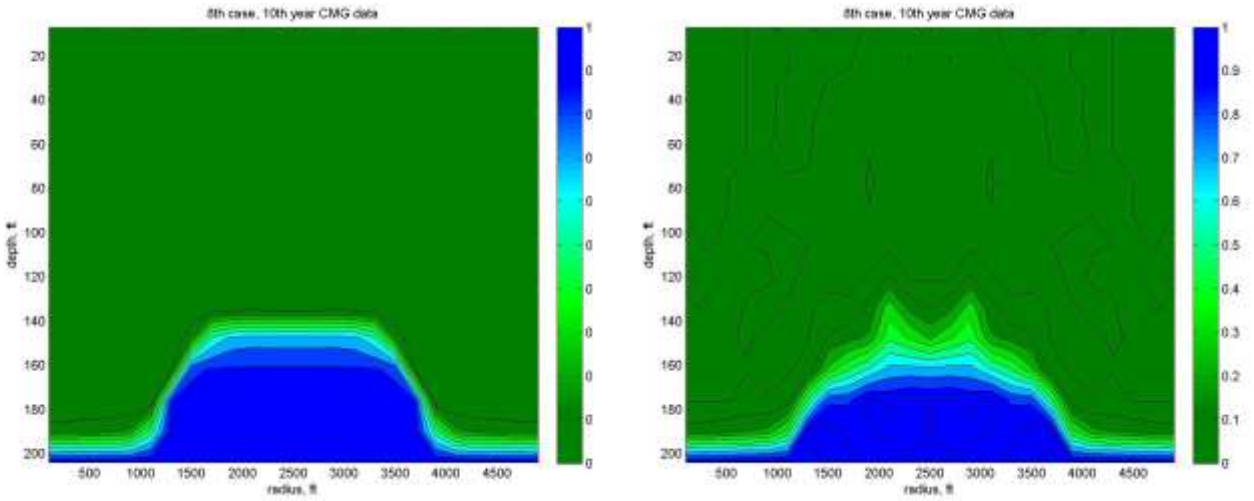

(a) Water saturation from numerical simulation

(b) Water saturation from artificial neural network

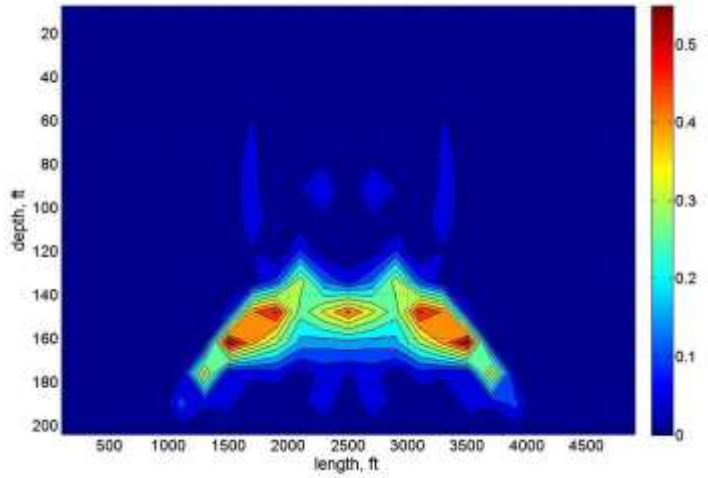

(c) Absolute error

Figure 6. Surface map of S_W for reservoir #10 at the end of the 10th year.

saturation data predicted from ANN. Figure 5c shows the absolute error of the ANN predicted water saturation for reservoir #8.

The ANN was able to predict the shape of water crest very effectively. There are areas which show an absolute error larger than 10%, but they are all at the bottom of the water cone which is not critical in performance calculations (Figure 5c). The more important areas are those which show where the water front has reached. The high error zones occur at the transition zones, similar to results of the vertical wells, and the high error occurs because saturation gradients are high over a small area, which creates a greater challenge to the ANN to predict the water saturation values accurately.

The second example to illustrate the ability of the ANN to predict the water coning phenomena is for reservoir #10. Figure 6a shows the surface map of water saturation for the reservoir with the numerical simulation data, and Figure 6b shows the surface map for the same reservoir with the ANN predicted data. The ANN was able to predict the cone shape, and also to predict the sharp decrease of water saturation at the bottom sides of the cone. Figure 6b shows two identical peaks. This is an overestimate of the water saturation values and this is because the horizontal section of the well, which is off the center, is having more flow than the center section. The ANN was successful in predicting this behavior, but the values of water saturation were overestimated. Figure 6c shows the absolute error of the ANN predicted water saturation for reservoir #10, and it

shows very low error (less than 10%) in most areas.

Conclusions

This study is concerned with predicting the rate of increase of water saturation in the immediate vicinity of the production wells using ANN based models. The developed ANNs are for vertical wells located in a radial flow geometry, and horizontal wells located in a rectangular reservoir system with active bottom water drives. A total of six input parameters are needed for the ANN to predict the water saturation distribution for a period of 10 years. The predicted water saturation values for the vertical well represent the water saturation distribution around the wellbore at the end of each year while the well is under production. In the case of horizontal wells, the water saturation predictions are made in the vertical plane of symmetry that cuts through the centerline of the horizontal well.

The examples of the applications described in this paper show that accurate saturation predictions matching the numerical simulation results effectively have been attained. With the help of the expert systems developed in this paper it will be possible to generate results showing the development of water saturation profiles as a function of time without resorting to reservoir simulators which require large amount of data and large computational times.

The developed ANNs can be used to optimize production strategies, by running the ANN under different production scenarios to find the production rate that will effectively delay water production. Furthermore, ANN based reservoir models developed in this study can be used in selecting the optimum perforation interval that will increase production of water-free oil by delaying water production or reducing it.

CONFLICT OF INTERESTS

The authors have not declared any conflict of interests.

REFERENCES

Al-Bulushi N, King PR, Blunt MJ, Kraaijveld M (2009). Development of artificial neural network models for predicting water saturation and flow distribution. Journal of Petroleum Science and Engineering 68:197-208.

Alimoradi A, Moradzadeh A, Bakhtiari MR (2011). Methods of water saturation estimation: Historical perspective. Journal of Petroleum and Gas Engineering 3(2):45-53.

Baziar S, Shahripour HB, Tadayoni M, Nabi-Bidhendi M (2018). Prediction of water saturation in a tight gas sandstone reservoir by using four intelligent methods: a comparative study. Neural ComputingandApplications30(4):1171-1185.

Blades A, Stright DH (1975). Predicting high volume lift performance in wells coning water. Journal of Canadian Petroleum Technology 14(4):61-70.

Byrne WB, Morse RA (1973). The effects of various reservoir and well parameters on water coning performance. In SPE Symposium on Numerical Simulation of Reservoir Performance, Houston, Texas, USA, 11-12 January.

Gharib H, Elsakka A, Chaw N (2018). Artificial neural network (ann) prediction of porosity and water saturation of shaly sandstone reservoirs. Advances in Applied Science Research 9:26-31.

Gholanlo HH, Amirpour M, Ahmadi S (2016). Estimation of water saturation by using radial based function artificial neural network in carbonate reservoir: A case study in sarvak formation. Petroleu, 2(2):166-170.

Hamada GM, Al-Gathe AA, Al-Khudafi AM (2015). Hybrid artificial intelligent approach for determination of water sat- uration using archie's formula in carbon- ate reservoirs. Journal of Petroleum and Environmental Biotechnology 6(6).

Helle HB, Bhatt A (2002). Fluid saturation from well logs using committee neural networks. *Petroleum* Geoscience 8:109-118.

Kuo MC (1983). A simplified method for water coning predictions. In SPE Annual Technical Conference and Exhibition, San Francisco, California, USA, 5-8 October.

Mahmoudi S, Mahmoudi A (2014). Water saturation and porosity prediction using back-propagation artificial neural network (bpann) from well log data. Journal of Engineering and Technology 5(2):1-8.

Mungan N (1975). A theoretical and experimental coning study. Society of Petroleum Engineers Journal 15(3):247-254.

Muskat M, Wyckoff HD (1935). An approximate theory of water coning in oil production. Transactions of the AIME 114(1):144-163.

Shokir EME-M (2004). Prediction of the hydrocarbon saturation in low resis- tivity formation via artificial neural net- work. In SPE Asia Pacific Conference on Integrated Modelling for Asset Management, Kuala Lumpur, Malaysia, 29-30 March.

Van T (1994). Water coning in a frac- tured reservoir. In SPE Annual Technical Conference and Exhibition, New Orleans, Louisiana, USA, 25-28 September.

Yang W, Wattenbarger RA (1991). Water coning calculations for vertical and horizontal wells. In SPE Annual Technical Conference and Exhibition, Dallas, Texas, USA, 6-9 October.

Zendehboudi S, Elkamel A, Chatzis I, Ahmadi MA, Bahadori A, Lohi A (2014). Estimation of breakthrough time for water coning in fractured systems: Experimental study and connectionist modeling. AIChE Journal 60(5):1905-1919.

Vol. 10(2), pp. 23-32, March 2019
DOI: 10.5897/JPGE2018.0303
Article Number: BEBB6A760369
ISSN: 2I41-2677

http://www.academicjournals.org/JPGE

ACADEMIC JOURNALS
expand your knowledge

Journal of Petroleum and Gas Engineering

Full Length Research Paper

Quantitative research on the influence of interlayer to thermal recovery horizontal wells in thick oil reservoir

Dong Liu*, Zong-Bin Liu, Jun-Ting Zhang, Jian-Min Zhu and Li-Lei Wang

Tianjin Branch of CNOOC Ltd., China National Offshore Oil Corporation, Tianjin 300459, China.

Received 2 November, 2018; Accepted 4 January, 2019

At present, the effect of different development patterns of interlayer like the length and the longitudinal position of interlayer on thermal recovery modes such as steam stimulation (CSS) and steam flooding (SF) is still a qualitative understanding, and there is no systematic study yet. Therefore, it is difficult to control the thermal production of thick oil reservoirs according to different interlayer patterns. In order to quantitatively analyze the influence of interlayer distribution pattern on steam huff and puff and steam flooding of horizontal wells in thick heavy oil reservoir, a numerical simulation model was established based on typical parameters of LD21 heavy oil reservoir in Bohai in China. Through comparison and research on the different modes of development longitudinal position, development length and development scale in non-permeable interlayer and semi-permeable interlayer. The influence of interlayer on the expansion law of steam chamber and ultimate oil recovery degree during steam huff and puff and steam flooding, and the main controlling factors of interlayer influencing oil recovery were obtained. The research results can be used for reference to optimize the location of thermal wells in thick heavy oil reservoir and reduce the influence of interlayer on thermal production effect of horizontal wells.

Key words: Heavy oil reservoir; interlayer; steam huff and puff; steam flooding; recovery.

INTRODUCTION

Interlayer mainly refers to the non-permeable or relatively low permeability band which can affect the seepage of oil and gas in the reservoir (WU et al., 2011). The stable interlayer can divide the thick reservoir into several relatively independent flow units. At present, injection steam for thermal recovery is the main way to improve oil recovery in heavy oil reservoirs (Wang et al., 2006; Zhu et al., 2011; Liu et al., 2012; Ajay, 2012; Huang et al., 2013; Khansari et al., 2014;Liu, 2015; Liu et al., 2015; Sheikholeslami et al., 2016; Hou et al., 2016; Yang et al., 2016; Ma and Liu, 2018; Zhong et al., 2015; Xiong et al., 2017). Interlayer affects fluid seepage by affecting the development and expansion of steam chamber (Zhou et al., 2006; Wang et al., 2009), which has a vital impact on the thermal effect of thick heavy oil reservoirs. Previous researchers have studied the quantitative identification criteria of different types of interlayer by using core data and logging data of coring wells. Through identification, interlayer can be divided into three types: shaly interlayer, calcareous interlayer and physical interlayer (Ma 2017; Yan and Duan, 2008). The stable distribution of interlayer is a positive significance to oil and gas development,

*Corresponding author. E-mail: liudong@cnooc.com.cn. Tel:+86 022 66500871.

Table 1. Fluid parameters of Guan IV Formation in LD21 heavy oil reservoir.

Parameter name	Parameter values	Parameter name	Parameter values
Buried depth of oil reservoir /m	1500	Thermal conductivity of upper and lower caprock / J• (m•day•C))$^{-1}$	1.06×10^{3}
Original average formation pressure /MPa	14.7	Reservoir temperature /℃	54
Rock compressibility /kPa^{-1}	2.5×10^{-5}	Vertical to horizontal permeability ratio	0.3
Volumetric heat capacity of rock /J• (m3•C)$^{-1}$	2.575×10^{6}	Reservoir thickness /m	42.9
Thermal conductivity of rock / J• (m•day•C))$^{-1}$	1.634×10^{5}	Average permeability of formation /m	3109
Thermal conductivity of oil / J• (m•day•C))$^{-1}$	9.77×10^{3}	Average porosity of formation	0.33
Thermal conductivity of water / J• (m•day•C))$^{-1}$	5.99×10^{4}	Degassing oil density / g•cm^{-3}	0.98
Thermal conductivity of gas / J• (m•day•C))$^{-1}$	1.9×10^{3}	Formation oil viscosity /mPa•s	2908
Volumetric heat capacity of upper and lower caprock /J• (m^{3}•C)$^{-1}$	2.2×10^{6}	Original oil saturation /%	62
Volumetric heat capacity of interlayer /J• (m^{3}•C)$^{-1}$	1.6×10^{6}	Thermal conductivity of interlayer / J• (m•day•C))$^{-1}$	0.55×10^{5}

such as the top interlayer can prevent steam overlap upward, the bottom interlayer can prevent bottom water coning and so on, while the unstable interlayer are surrounded by more residual oil distribution, which is not conducive to development (Zhong, 2012). Some scholars take actual oilfield as an example to study the influence of interlayer on development effect in the process of steam huff and puff, steam flooding after huff and puff, steam-assisted gravity drainage, and obtain the qualitative understanding of interlayer on thermal effect (Tang, 1995; Li, 2016). Generally speaking, the study on the effect of interlayer on thermal horizontal wells is not very detailed; the range of interlayer is a qualitative understanding, which cannot meet the requirement of CSS and SF. In CSS and SF process, interlayer length and interlayer longitudinal position are very important in thick heavy oil reservoirs, which can decide the well location. In order to quantitatively analyze the influence of interlayer distribution pattern on steam huff and puff and steam flooding of horizontal wells in thick heavy oil reservoir, longitudinal position, development length and development scale in non-permeable interlayer and semi-permeable interlayer were researched. The research results can be used for reference to optimize the location of thermal wells in thick heavy oil reservoir and reduce the influence of interlayer on thermal production effect of horizontal wells.

The establishment of theoretical model

The main oil-bearing layer of LD21 heavy oil reservoir is Guantao Formation in Bohai, of which Guan IV Formation is a layered edge water reservoir with high oil viscosity (formation oil viscosity 2908 mPa·s), deep reservoir (1500 m), good reservoir physical properties (logging porosity 33.2%, logging permeability 2145mD), thick reservoir (single layer thickness 16 ~ 40 m). The energy of water is stronger (volume multiplier of water to oil is 4~11 times). By analyzing the geological reservoir characteristics of Guan IV Formation of LD21 heavy oil reservoir in Bohai oilfield, a basic model is established without interlayer. The fluid parameters and geological parameters used in the model are shown in Table 1.

Using the STARS simulator of CMG software, the grid size in *I* and *J* directions are both 20m and is 1.3m in *K* direction in the model. The number of grids in *I* direction and *J* direction is 23 and 20, respectively. The number of grids in *K* direction is 33. The total number of simulated grids is 23×20×33=15180. Longitudinally, it is composed of a set of oil layers. The 1st to 33rd layers are oil layers from top to bottom. The effective thickness of oil layers is 42.9 m. Three horizontal wells are located in the middle of the reservoir, 100m from the edge, perforation length of horizontal section t is 300m, and the well spacing is 200 m (Figure 1).

Three wells are injected steam huff and puff at the same time. The daily steam injection rate of a single well is 300 m^{3}/d, the cyclic steam injection is 4500 m^{3}, the bottom hole steam injection temperature is 340°C, the bottom hole steam quality is 0.4, keep the wells shut for 5 days after steam injection. Oil wells are simulated by three-stage control conditions: the first control condition is constant maximum liquid (150m^{3}/d), the second control condition is constant pressure drop (4 MPa), and the third control condition is constant minimum bottom flow pressure (3 MPa). Simulated two production processes: three wells injected steam huff and puff for seven rounds at the same time, and then the intermediate horizontal well H2 changed for steam injection, a single well daily steam injection is 300 m^{3}/d, bottom hole steam injection temperature is 340°C, bottom hole steam quality is 0.6. This model can be used for injection steam development of the well pattern of 1 injection 2 production; the well is

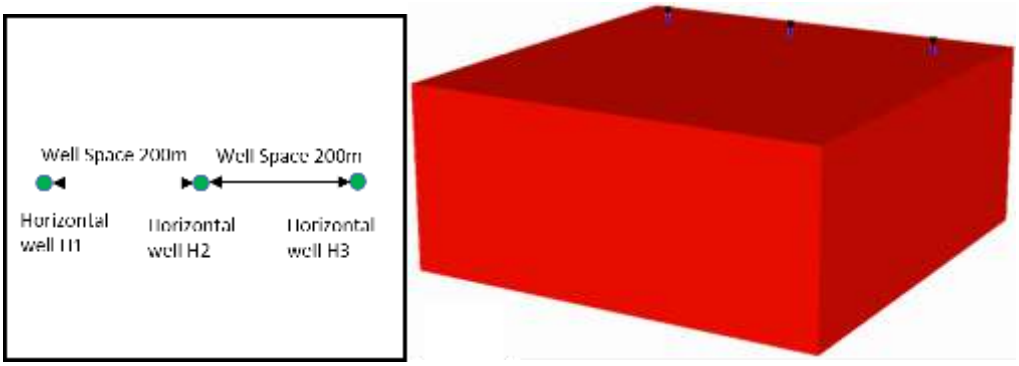

Figure 1. Schematic diagram of a typical well group numerical model I for (a) well location, (b) Original oil saturation field (S_{oi}=0.62).

Table 2. Numerical simulation design.

influence factors	Whether interlayer distributed	Specific value	Test Number
Vertical position of horizontal well	No	Upper part , middle part, Lower part	6
Non dimensional position of interlayer	Yes	0.13, 0.25, 0.38, 0.50, 0.63, 0.75,0.88,1.00	16
Non dimensional length of interlayer	Yes	0.06,0.18,0.29,0.41,0.53,0.65,0.76	14
Development scale of interlayer	Yes	Whole region distribution, Upper local distribution, Lower local distribution	6

shut-in until the entire oil field's instantaneous oil-gas ratio is below 0.15 (Table 2).

The design of test scheme

The permeability of different lithologic interlayers varies greatly, and the mudstone type has the strongest ability to seal fluid (vertical permeability is less than $1\times10^{-3}\mu m^2$), the calcareous sandstone type is next (vertical permeability is less than 2×10^{-3} μm^2), and the mixed sandstone and oil stain sandstone have the worst ability to seal fluid (vertical permeability is less than 60×10^{-3} μm^2) (Tang, 1995). The type of interlayers used in this paper is non-permeable and semi-permeable, and the corresponding permeability is 0.000×10-3 μm^2 and 0.001×10^{-3} μm^2 respectively. The schema is shown in Table 2.

The dimensionless position of interlayer is defined as the vertical distance between interlayer and horizontal well divided by the distance between horizontal well and reservoir top. The expression is as follows:

$$D_{Dm} = D_1 / D_H \quad (1)$$

In the formula, D_1 is for the vertical distance between the interlayer and the horizontal well, m; D_H is for the vertical distance between the horizontal well and the top of the reservoir, m.

The dimensionless length of the interlayer is defined as the length of the interlayer divided by the length of the reservoir in the plane. The expression is as follows:

$$L_{Dm} = L_1 / L_H \quad (2)$$

In the formula, L_1 is the length of the interlayer, m; L_H is the length of the reservoir, m.

Analysis of heating chamber expansion rule and development effect

Based on the above models and schemes, the development effects of steam huff and puff and steam flooding after steam huff and puff under different modes, such as vertical position of horizontal wells, dimensionless position of interlayer, and dimensionless thickness of interlayer and interlayer development scale

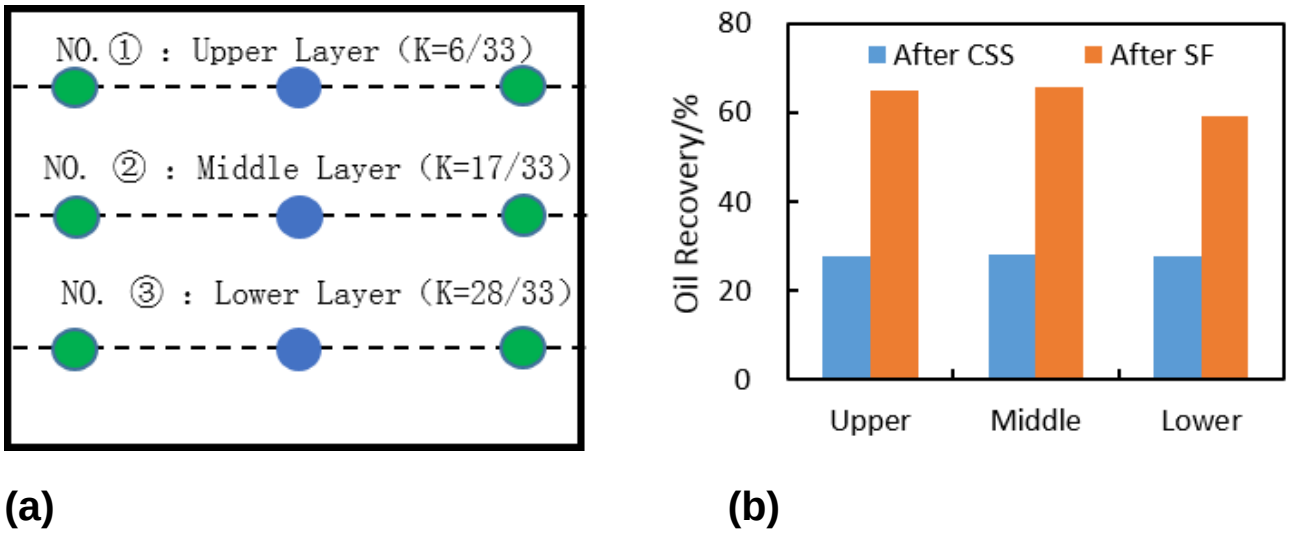

Figure 2. Influence of vertical position of horizontal well for (a) vertical location diagram, (b) development indicator diagram of different locations.

are researched respectively.

The influence of vertical position of horizontal wells

In order to determine the basic model, the best well location of thick and heavy oil reservoirs without interlayer development is researched. As shown in Figure 2a, three horizontal wells are deployed in the upper, middle and lower parts of the reservoir to obtain the oil recovery at the huff and puff stage and at the end of displacement, as shown in Figure 2. The results show that when the three wells are located in the middle of the reservoir simultaneously, the recovery degree of huff and puff stage and steam flooding stage reaches the maximum of 28.1% and 65.8%.

Dimensionless position of interlayer

The distance of interlayer and the vertical position of horizontal well affect the distribution and expansion of steam, and ultimately affects the heating range and oil displacement range, thus affecting the thermal recovery effect. Figure 3 is a comparison of the temperature field at the end of steam flooding after huff and puff at different interlayer positions (K = 13/33, K = 9/33, K = 5/33), the corresponding dimensionless interlayer positions (0.25, 0.50, 0.75).

Figure 3 shows that the non-permeable interlayer and permeable interlayer have different effects on the heating range. As shown in Figure 3a, for such non-permeable interlayer as argillaceous interlayer, it is difficult for the injected steam to enter the upper part of the interlayer, resulting in a lower temperature in the upper part of the interlayer at the end of development. For such semi-permeable interlayer as physical interlayer, the injected steam can heat the upper part of the interlayer, and the temperature increases significantly at the end of development, as shown in Figure 3b. It can be seen that for heat conduction and convection, the semi-permeable interlayer slows down the heat transfer, and the heat transfer performance is better than the non-permeable interlayer.

Figure 4 compares the remaining oil saturation at the end of steam flooding development at different interlayer positions. As shown in Figure 4a, for a non-permeable interlayer, there is obvious residual oil accumulation area at the upper part of the interlayer, indicating that the interlayer prevents fluid flow in the upper part of the interlayer. For a semi-permeable interlayer, the upper part of the interlayer is available, showing that the remaining oil saturation is lower than the original oil saturation, as shown in Figure 4b. It can be seen that the reservoirs located at the upper and lower parts of the semi-permeable interlayer can contribute to the oil production.

Figure 5 is a development index for different interlayer positions. Figure 5a shows that with the increase of dimensionless position of interlayer, the recovery degree increases gradually in huff and puff stage. Figure 5b shows that the recovery degree increases first and then decreases at the end of steam flooding whether it is non-permeable interlayer or semi-permeable interlayer. When the development position of interlayer changes from K=13/33 to K=5/33, the oil recovery degree of CSS increases from 26.3 to 27.7%. For steam flooding, the final recovery degree tends to be consistent.

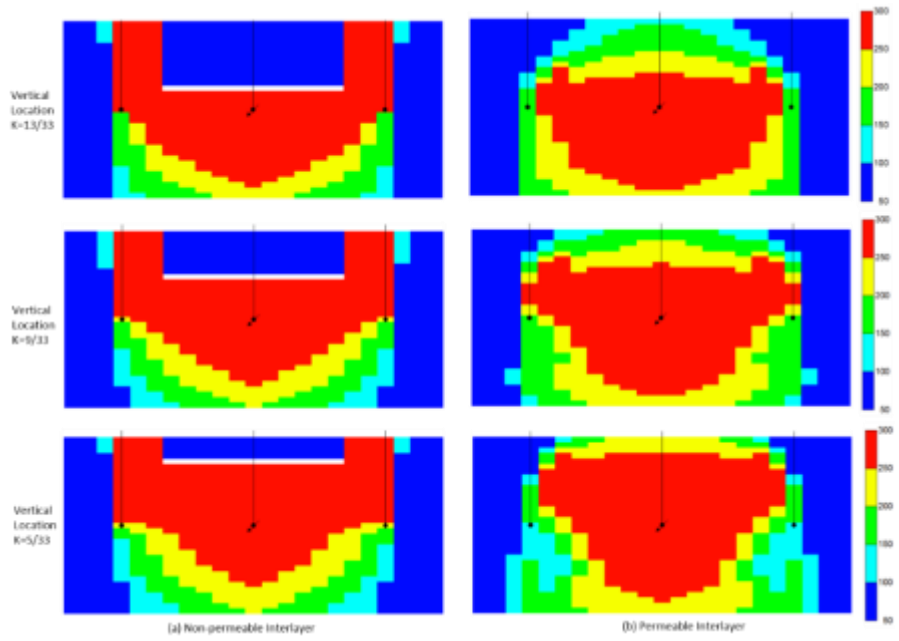

(a) **(b)**

Figure 3. Temperature field at the end of steam flooding of different interlayer locations for (a) Non-permeable Interlayer, (b) Permeable Interlayer. The red area is heated oil, the blue area is not heated oil.

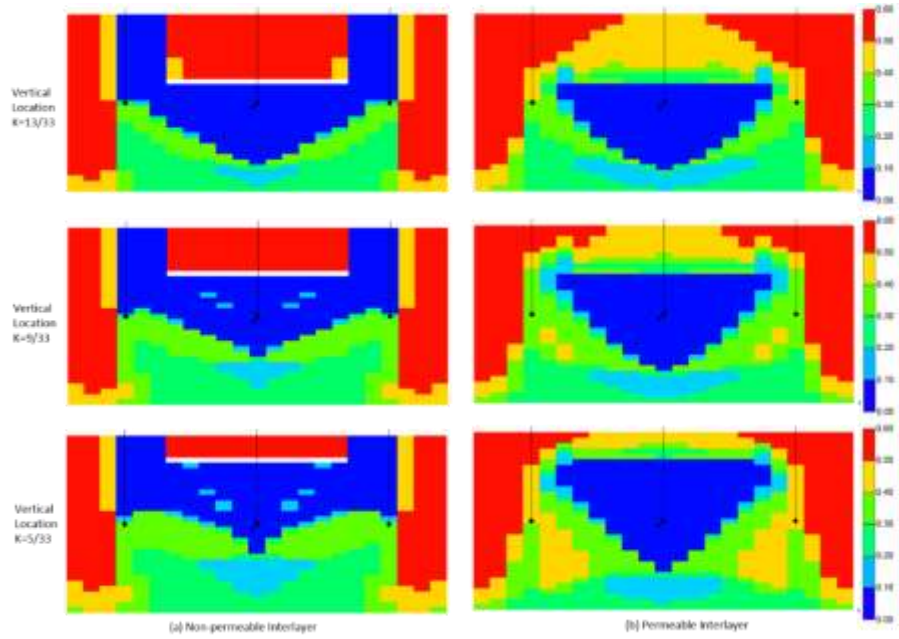

(a) **(b)**

Figure 4. Remaining oil saturation field at the end of steam flooding of different interlayer locations for (a) Non-permeable Interlayer, (b) Permeable Interlayer. The blue area is less remaining oil saturation, the red area means larger remaining oil saturation.

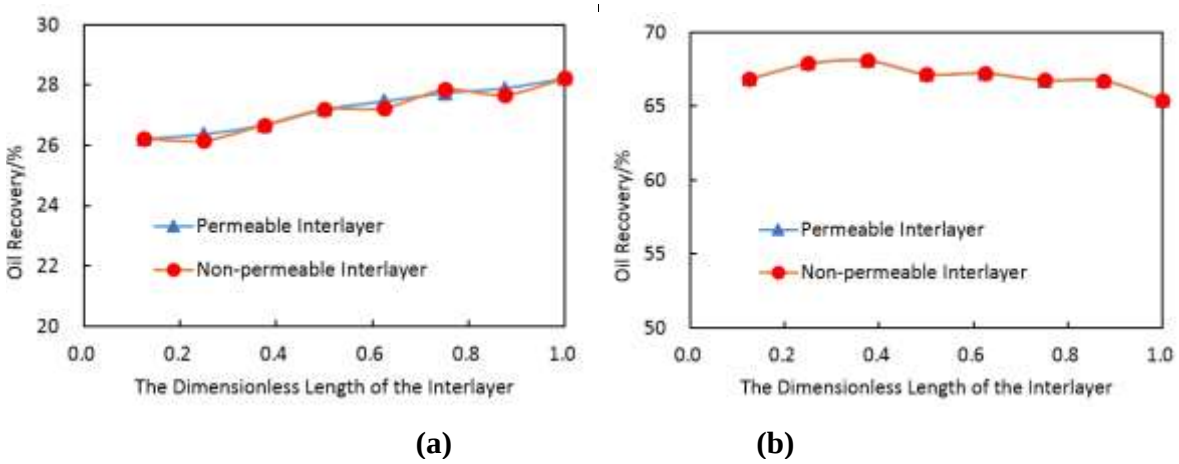

Figure 5. Development indicators of different interlayer locations for (a) cycle steam stimulation for 7 cycle, (b) after steam flooding.

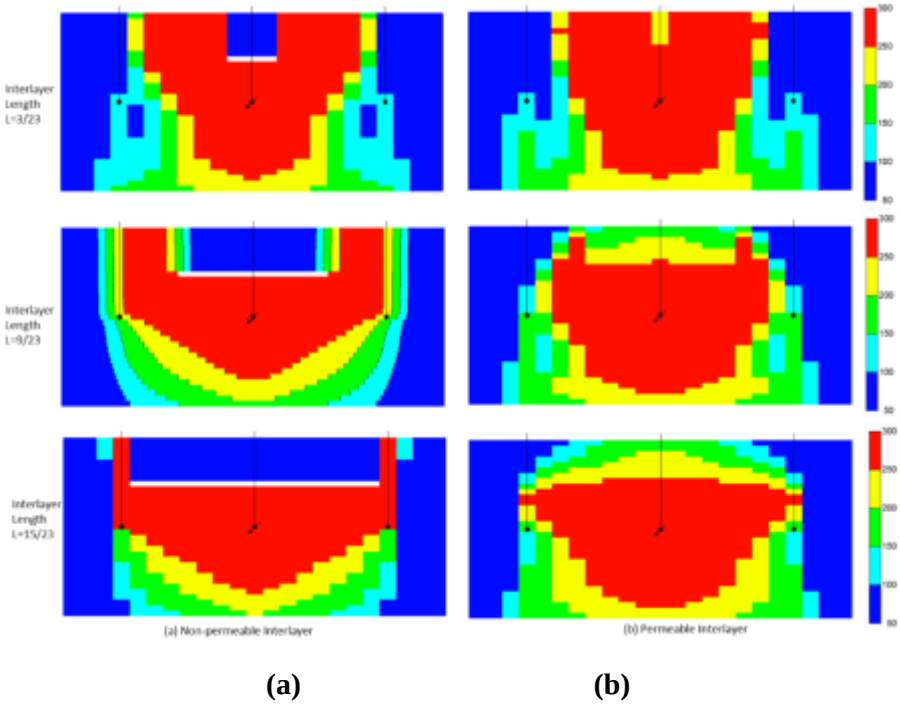

Figure 6. Temperature field at the end of steam flooding of different interlayer lengths for (a) Non-permeable Interlayer, (b) Permeable Interlayer. The red area is heated oil, the blue area is not heated oil.

The dimensionless length of interlayer

The dimensionless length of interlayer affects the distribution and expansion of steam, and affects the heating range and oil displacement range, thus affecting the thermal recovery effect. Figure 6 is a comparison chart of temperature field at the end of steam drive after huff and puff with different interlayer lengths (L= 3, L= 9, L= 15), corresponding dimensionless interlayer lengths (0.18, 0.53, 0.88).

Figure 6 shows that the longer the interlayer develops, the more obvious the compression of the heating range and the wider the lateral expansion range of the steam injection. When the interlayer is short, the injected steam

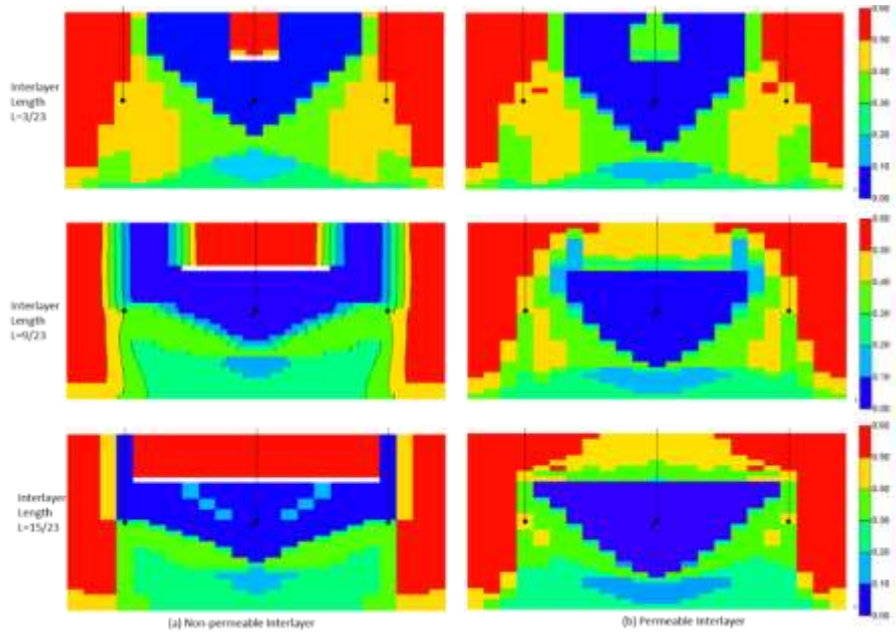

(a) **(b)**

Figure 7. Remaining oil saturation field at the end of steam flooding of different interlayer lengths for (a) Non-permeable Interlayer, (b) Permeable Interlayer. The blue area is less remaining oil saturation, the red area means larger remaining oil saturation.

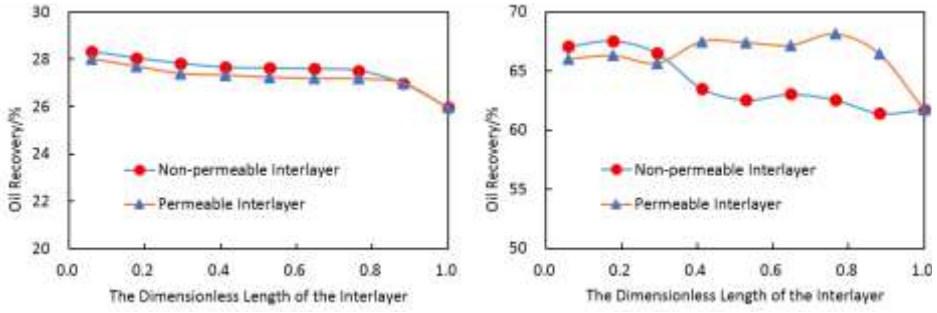

(a) **(b)**

Figure 8. Development indicators of different interlayer lengths for (a) cycle steam stimulation for 7 cycle, (b) after steam flooding 4.4 development scale of interlayer.

mainly extents to the top of the reservoir and then expands laterally; when the interlayer is long, the injected steam quickly reaches the top of the interlayer, and then expands laterally, increasing the lateral sweep volume. For non-permeable and semi-permeable interlayer, the vertical sweep coefficient of semi-permeable interlayer is higher, while the transverse sweep range is smaller. The difference of heating mode will lead to the difference between the seepage law of oil and the distribution of remaining oil.

Figure 7 compares the remaining oil saturation field at the end of the development of steam drive with different interlayer lengths. As shown in Figure 7a, for a non-permeable interlayer, there is obvious residual oil accumulation area at the upper part of the interlayer, indicating that the interlayer prevent fluid flow in the upper part of the interlayer. For a semi-permeable interlayer, the upper part of the interlayer is available, as shown in Figure 7b.

Figure 8 is a development index for different interlayer lengths. Figure 8a shows that with the increase of dimensionless length of interlayer, the recovery degree

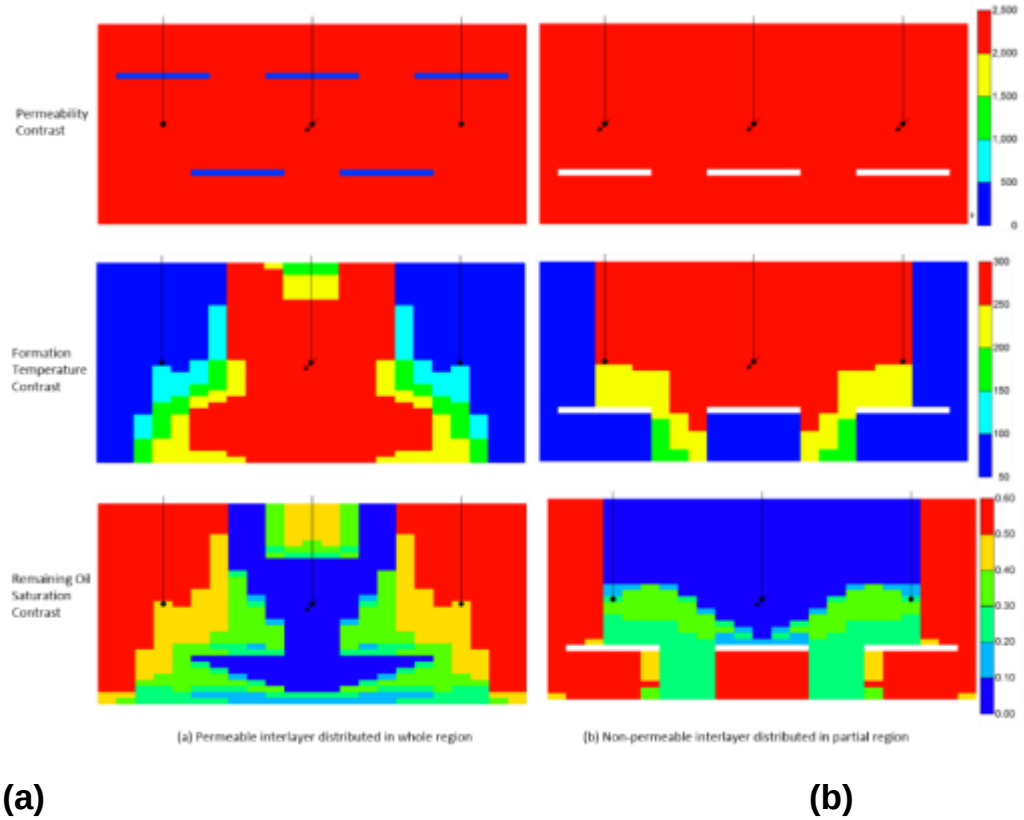

Figure 9. Permeability, formation temperature, remaining oil saturation field diagram comparison at the end of steam flooding of different interlayer development scales for (a) Permeable interlayer distributed in whole region, (b) Non-permeable interlayer distributed in partial region.

decreases gradually in huff and puff stage whether it is non-permeable interlayer or semi-permeable interlayer. When the dimensionless length of interlayer increases from 0.06 to 1.00, the recovery degree decreases from 28.3 to 26.0% during huff and puff stage. For steam flooding after huff and puff, the recovery degree of semi-permeable interlayer decreases from 67.5 to 61.7%, while the recovery degree of non-permeable interlayer first decreases and then keep stable.

Figure 9 is a comparison of permeability field, formation temperature field and residual oil saturation field of different interlayer development scale. It can be seen that the different development scale of interlayer affects the distribution of temperature field and remaining oil saturation field. Figure 10 (a) shows that for huff and puff development, the recovery degree of non-permeable interlayer is slightly higher than permeable interlayer. The main reason is that the heating range of huff and puff is limited, and the influence of interlayer is not obvious. However, with the development of production, the recovery degree of non-permeable interlayer is lower than permeable interlayer while steam flooding after huff and puff. Especially when the interlayer is distributed at the bottom or in the whole area, the difference of recovery degree between them is 3.2-3.8%.

The influence of interlayer development on well location design

In the case of interlayer distributed in the whole area, there are three well distribution modes: 1) vertical well passes through one set of interlayer; 2) directional well obliquely passes through two sets of interlayer; 3) horizontal well deployed between two sets of interlayer, as shown in Figure 11.

Table 3 is the recovery degree of huff and puff stages and the end of steam drive at different well location pattern. Table 3 shows that the more passing through the interlayer, the better the development effect for directional well development. The recovery degree of directional well passing through two sets of interlayer is higher than that vertical well passing through one set of interlayer. Directional well can get 5.6 percentage point and 3.4 percentage point higher oil recovery than that of vertical well for huff and puff and steam flooding, respectively. Horizontal wells have the best recovery effect, and the recovery degree can reach 28.9% in huff

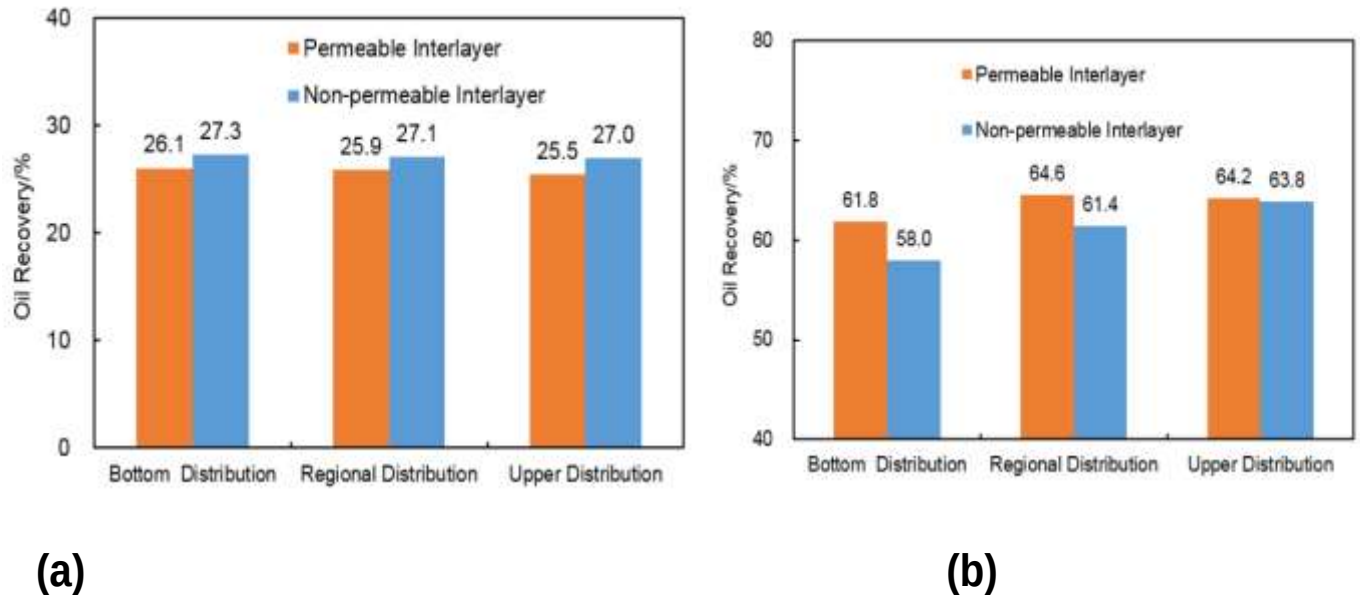

Figure 10. Development indicators of different interlayer models for (a) cycle steam stimulation for 7 cycle, (b) after steam flooding.

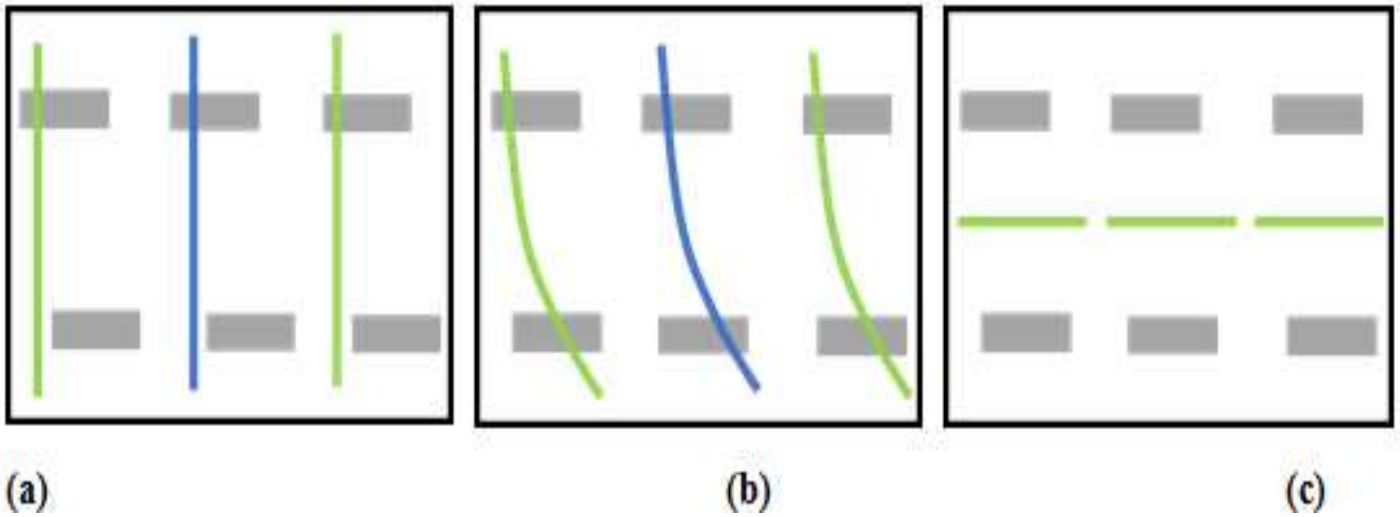

Figure 11. Different well type of interlayer distributed in whole region for (a) vertical well, (b) directional well, (c) horizontal well.

Table 3. Comparison of recovery degree for different well pattern of interlayer distributed in the whole area.

Case name	Pass through interlayer	Steam injection rate	Injection-production ratio	Huff and puff stage recovery degree	Steam drive end recovery degree	Recovery degree added value
	/	/ (m^3/d)	/	/%	/%	/%
Vertical well	Pass through one set of interlayer	300	1.2	15.0	43.5	/
Directional well	Pass through two sets of interlayer	300	1.2	20.6	46.9	3.4
Horizontal well	Not pass through interlayer	300	1.2	28.9	59.7	16.2

and puff stage, 59.7% at the end of steam flooding. It can get 13.9 percentage point and 16.2 percentage point higher oil recovery than that of vertical well for huff and puff and steam flooding, respectively.

CONCLUSION AND RECOMMENDATIONS

(1) When there is no interlayer, the horizontal wells are located in the middle of the reservoir, the recovery degree of the huff and puff stage and steam drive stage reaches the maximum of 28.1% and 65.8% respectively. Therefore, it is suggested that thermal recovery horizontal wells should be deployed in the middle part of reservoirs for the reservoir of no interlayer.
(2) Mudstone interlayer (non-permeable interlayer) and physical interlayer (semi-permeable interlayer) have different effects on thermal recovery. For the semi-permeable interlayer, the upper part of the interlayer can be developed, but the non-permeable interlayer cannot be developed.
(3) With the increase of dimensionless position of the interlayer, the recovery degree increases gradually in huff and puff stage, and the recovery degree increases first and then decreases at the end of steam flooding whether it is non-permeable interlayer or semi-permeable interlayer.
(4) The longer the interlayer develops, the more obvious the compression of the heating range and the wider the lateral expansion range of the steam injection. When the dimensionless length of interlayer increases from 0.06 to 1.00, the recovery degree decreases from 28.3 to 26.0% during huff and puff stage. For steam flooding, the recovery degree of physical interlayer decreases from 67.5 to 61.7%.
(5) For two sets of discontinuous interlayers, horizontal wells are the best, directional wells are the second and vertical wells are the worst. For directional wells, the more interlayers are passed through by directional wells, the effect is the better.

CONFLICT OF INTERESTS

The authors have not declared any conflict of interests.

ACKNOWLEDGEMENT

This work was supported by the National Science and Technology Major of China (2016ZX05058-001-008), which was named optimization and application of thermal recovery in offshore heavy oil fields.

REFERENCES

Ajay M (2012). Modified analytical model for prediction of steam flood performance. Journal of Petroleum Exploration and Production Technology 2:117-123.

Huang YH, Liu D, Luo YK (2013). Research on multiple thermal fluid stimulation for offshore heavy oil production. Special Oil and Gas Reservoirs 20(2):164-165.

Xiong H, Huang S, Liu H (2017). A Novel model to investigate the effects of injector-producer pressure difference on SAGD for bitumen recovery. International Journal of Oil, Gas and Coal Technology 16(3):17-235.

Hou J, Zhou K, Zhao H, Kang XD, Wang ST, Zhang XS (2016). Hybrid optimization technique for cyclic steam stimulation by horizontal wells in heavy oil reservoir. Computers & Chemical Engineering 84(4):363-370.

Khansari Z, Kapadia P, Mahinpey N, Gates ID (2014). A new reaction model for low temperature oxidation of heavy oil: Experiments and numerical modeling. Energy 64:419-428.

Li W (2016). The influence of interlayer on the development effect of the vertical and horizontal wells SAGD. Science Technology and Engineering 16(4):28-32.

Liu D, Li YP, Zhang FY (2012). Reservoir applicability of steam stimulation supplemented by flue gas. China Offshore Oil and Gas 24(S1):62-66.

Liu D (2015). A new model for calculating heating radius of thermal recovery horizontal wells. China Offshore Oil and Gas 27(3):84-90.

Liu D, Hu TH, Pan GM (2015). Comparison of production results between multiple thermal fluid huff and puff and steam huff and puff in offshore application. Special Oil and Gas Reservoirs 22(4):118-120.

Sheikholeslami M, Hayat T, Alsaedi A (2016). Numerical analysis of EHD nanofluid force convective heat transfer considering electric field dependent viscosity. International Journal of Heat and Mass Transfer. 108:2558-2565.

Ma KQ, Liu D (2018). Model for capacity forecasting of thermal soaking recovery in horizontal wells in heavy oil reservoirs. Journal of Southwest Petroleum University (Science and Technology Edition) 40(1):114-121.

Ma CL (2017). Classification and identification of the interlayer in block D of medium-thick viscous oil reservoirs in Liaohe Oilfield. Journal of Geology 41(2):342-346.

Tang QSX (1995). Characteristics of partings and their effects on thermal recovery of heavy oil of GAO 3 area in Gaosheng oilfield. Special Oil and Gas Reservoirs 2(1):23-30.

Wang GY, Yang SC, Liao FY (2009). Hierarchical structure of barrier beds and interbeds in braided river reservoirs. Natural Gas Geoscience 20(3):378-383.

Wang S, Huang Y, Civan F (2006) Experimental and theoretical investigation of the Zaoyuan field heavy oil flow through porous media. Journal of Petroluem Science and Engineering 50:83-101.

Wu Y, Li M, Cui Z (2011). Effect of interbeds within the thick debouch bar sand body on remaining oil distribution. Journal of Yangtze University (Natural Science Edition) 8(3):58-60.

Yan YZ, Duan TX (2008). Identification and inter-well prediction of interbeds in thick oil layer. Lithologic Reservoirs 20(2):127-131.

Yang Y, Huang SJ, Yang L, Song QL, Wei SL, Xiong H (2016). A multistage theoretical model to characterize the liquid level during steam-assisted-gravity-drainage process. SPE Journal 22(01):327-338.

Zhou GW, Tan CQ, Zheng XW (2006). Research on recognition of barrier/interbed via logging in H Oilfield. Geophysical Prospecting for Petroleum 45(5):542-545.

Zhong YL (2012). The Significance of interlayer in thermal recovery of heavy oil by steam stimulation. Journal of Shengli College China University of Petroleum 26(4):6-8.

Zhong LG, Tian YC, Jiang YX (2015). Low temperature oxidation reaction of super heavy oil in block Du 84 of Liaohe Oilfield. Journal of Northeast Petroleum University 39(2):116-122.

Zhu J, Li CX, Xin PG (2011). Analysis of viscosity-temperature characteristics and rheology behavior for heavy oil. Journal of Petrochemical Universities 24(2):66-68.

Related Journals: